Sports Engineering (2022) 25:26
https://doi.org/10.1007/s12283-022-00390-5

ORIGINAL ARTICLE

Disc golf trajectory modelling combining computational fluid dynamics and rigid body dynamics

Knut Erik Teigen Giljarhus[1] · **Mika Tobias Gooding**[1] · **Joar Njærheim**[1]

Accepted: 25 October 2022

Abstract
In the sport of disc golf, athletes utilize discs with various shapes to achieve their desired throws. Computational methods have the potential to give further insight into how the disc shape and throw parameters influence the disc trajectory. A methodology is presented that combines computational fluid dynamics to obtain the aerodynamic coefficients for a given disc shape, with rigid body dynamics to simulate the disc golf flight. The computational fluid dynamics simulations were performed in OpenFOAM, and compared against wind tunnel experiments from the literature. The trajectory model was implemented in an open-source software, and compared against simulated trajectories against measured trajectories of actual disc golf throws. The methodology was applied to three different discs, comparing their aerodynamic coefficients and flight trajectories. How the disc shape impacts lift, drag and moment coefficients and corresponding flight trajectories is discussed. The methodology has the potential to consistently characterize the flight of a disc and lead to greater understanding of disc flight, and thereby contribute to both training, disc development and regulation.

Keywords Simulation · Sports projectiles · Aerodynamics

1 Introduction

Disc golf is a sport where the players throw discs at a target, with rules similar to golf. In recent years, the sport has seen significant growth [1, 2]. From a sports engineering and aerodynamics perspective, the sport is interesting as it is arguably the sport with the broadest range of projectile shapes. Compared to other sports, where typically only one projectile is used, a disc golf athlete can carry more than twenty different discs in a competition. The choice of disc for a particular throw depends on the distance to the target, obstacles on the way to the target and wind conditions. The sport was made possible by utilizing discs with a triangular rim [3]. This design yielded improved aerodynamics compared to former flying discs, such as the Frisbee [4], and the increased amount of mass in the rim gives it increased gyroscopic stability, which is crucial for control in a sports setting. The current technical standards [5] for disc design gives a large amount of flexibility, leading to a high number of manufacturers with a wide range of designs. The current methodology for determining the flight characteristics uses a rating system with four numbers; speed, glide, turn and fade. However, the system is subjective, with no standard way of determining the numbers. Scientific methods, such as experimental testing, computational analysis and mathematical models, have the potential to consistently characterize the flight of a disc. Such studies can also lead to greater understanding of disc flight, and thereby contribute to both training and disc development.

The scientific studies on disc golf flight are relatively sparse, with much of the available literature focusing on Frisbee-like geometries. In Ref. [6], a comprehensive experimental study on the aerodynamic characteristics of a Frisbee was performed. Results were found to be independent of Reynolds number, and spin did not significantly influence the aerodynamic coefficients for typical spin ratios. The

Open access funding provided by University Of Stavanger.

This article is a part of a Topical Collection in Sports Engineering on The Engineering of Sport 14 Conference held at Purdue University USA, edited by Dr Hugo Espinosa, Steven Shade, Dr Kim Blair and Professor Jan-Anders Månsson.

✉ Knut Erik Teigen Giljarhus
knut.e.giljarhus@uis.no

[1] Department of Mechanical and Structural Engineering and Materials Science, Faculty of Science and Technology, University of Stavanger, PB 8600, 4036 Stavanger, Norway

Published online: 16 November 2022

negligible influence of spin was also confirmed in Ref. [7] using computational fluid dynamics (CFD) simulations. The investigation in Ref. [6] was later extended to discs with triangular rims in Ref. [8]. In Refs. [9, 10], CFD simulations were performed for flying discs and compared against the experiments of Ref. [8], with reasonable agreement in aerodynamic coefficients. In addition to wind tunnel experiments and CFD simulations, there are also examples on using onboard instrumentation to both track the flight and estimate aerodynamic coefficients [11–13]. In Ref. [14], a kinematic model was developed for Frisbee flight and combined with flight trajectory experiments to estimate aerodynamic coefficients. The kinematic model was based on Newton-Euler equations for rigid bodies. A similar model was used in Ref. [15] to investigate the influence of initial disc launch parameters on the Frisbee flight.

This work combines CFD simulations to obtain the aerodynamics properties of a disc with rigid body dynamics to simulate the flight of disc golf discs. A computational methodology for determining the aerodynamic coefficients is presented, along with an open-source flight trajectory model to simulate the disc golf flight. The CFD model is compared against available wind tunnel data [8], while experiments are performed to assess the accuracy of the trajectory model.

2 Methods

2.1 Disc geometries

The disc geometry was obtained by using a side profile image to trace the outer shape and using an Artec Eva 3D scanner in HD mode to trace the inner rim. A spline was created from a slice of the disc, which was then revolved to create a 3D model. The moments of inertia are also needed by the rigid body dynamics model, and were found directly from the 3D geometry file using the `trimesh` Python library.

Figure 1a shows the side profile of the discs used in this work. The discs are commercial discs in Star plastic from Innova (Innova Champion Discs Inc., California, United States), namely a distance driver of model Wraith (DD), and two control drivers of models Firebird (CD) and Roadrunner (CD2).

Discs are typically made from plastic using injection molding. Due to variability in plastics, and also production conditions such as temperature and humidity, there can be slight differences in the disc shape and dimensions that can influence the aerodynamic performance. Figure 1b shows an image of the nose of two DD discs used in the flight trajectory experiments. It is evident that the height to the leading edge is different in the two discs, with a difference of about 3 mm, which will influence the flight. For the experiments, multiple discs were used for repeated throws, and the discs were visually inspected to ensure they had only minor differences in shape.

2.2 Computational fluid dynamics

CFD simulations are performed using the open-source OpenFOAM CFD software [16, 17]. The SIMPLE method was used for pressure-velocity coupling, and turbulence was modelled using the k-omega shear stress transport (SST) model [18].

Second-order discretization schemes were used for all variables, and in particular the second-order linear upwind scheme was used for the convective terms [19].

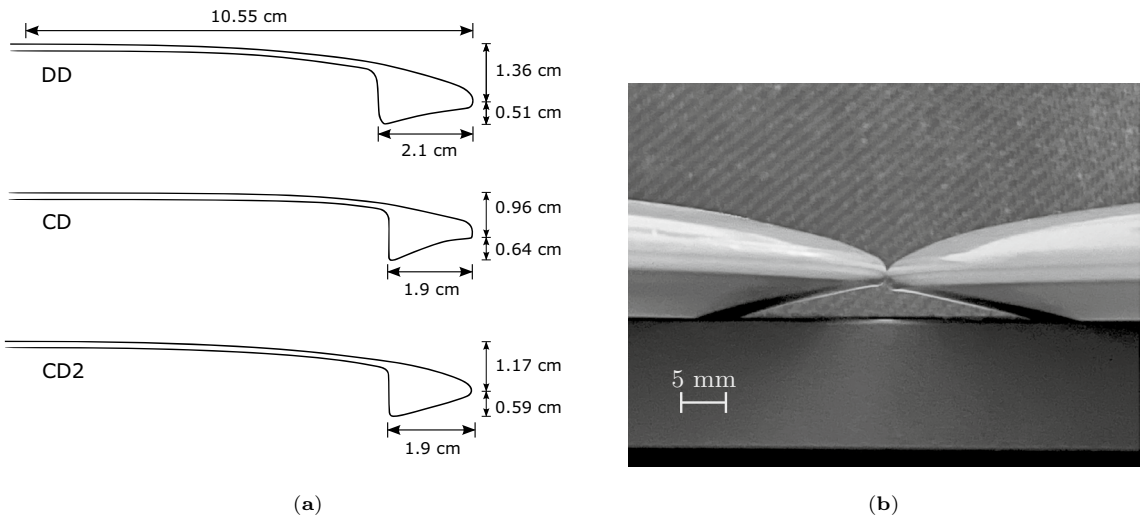

Fig. 1 **a** Side profile of discs with specifications. **b** Illustration of difference in flight plate height for two DD discs

The computational domain was a rectangle with dimensions $20D \times 10D \times 10D$, where D is the disc diameter. The disc was placed in the center, $5D$ from the inlet. The disc was kept fixed in the simulations, as spin has been shown to have negligible influence on the aerodynamic coefficients [6, 7]. The inlet velocity was set to 26.9 m/s, which corresponds to a disc Reynolds number of 3.78×10^5. The Reynolds number is defined as $Re = UD/\nu$, where U is the inlet velocity and ν is the kinematic viscosity of air. At the outlet a fixed value of zero for pressure was used and zero gradient conditions for the remaining fields. Slip conditions were applied at the sides.

The mesh is illustrated in Fig. 2. A new mesh was generated for each angle of attack, ensuring cells are aligned with the flow and yielding high resolution in the wake. A total of 7 2:1 refinement levels were used towards the disc surface, giving a cell size of 0.3 mm in the vicinity the disc. Additionally, 15 prism layers were inserted near the surface to resolve the boundary layer, with a minimum size of 20 µm and an expansion ratio of 1.2. This gave a maximum y^+ value less than 2 and an average y^+ value less than 0.5 for all cases. The total grid size was about 23 million cells. The simulation was performed for 6000 iterations, after which the scaled residuals for the equations and the variations in aerodynamic coefficients were below 1×10^{-4}.

The forces on the disc were calculated by integrating the pressure contribution and the viscous contribution over the disc surface. From this the aerodynamic coefficients were calculated using the following standard definitions:

$$F_D = qC_DS \tag{1}$$

$$F_L = qC_LS \tag{2}$$

$$M = qC_MDS \tag{3}$$

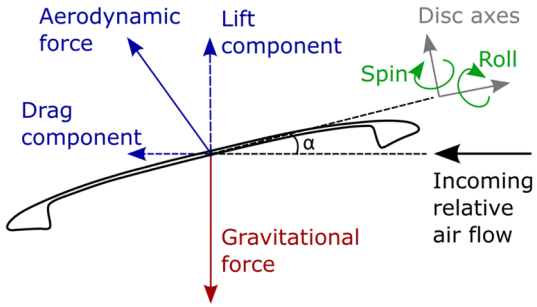

Fig. 3 Illustration of forces acting on the disc

where C_D, C_L and C_M denote the drag, lift and pitching moment coefficients, respectively. $q = 0.5\rho U^2$ is the dynamic pressure and S is the disc planform area.

2.3 Rigid body dynamics

The rigid body dynamic model is based on flight vehicle dynamics [20] and previous work on disc trajectory modelling [14, 15].

The disc is described by a location vector, $\boldsymbol{x} = (x, y, z)$ and an attitude vector using Euler angles, $\boldsymbol{\theta} = (\phi, \theta, \psi)$.

By using a series of coordinate transformations (see Appendix A and Online Resource 1), the equations of motion can be written in a straight-forward manner, directly using the aerodynamic force coefficients calculated in the CFD simulations. The four coordinate systems are,

1. **Earth axes** - fixed coordinate system with the origin placed at the ground of the position for the release of the disc.
2. **Disc axes** - coordinate system moving with the disc, found by translation of the location vector and a sequence of rotations defined by the attitude vector.
3. **Zero sideslip axes** - coordinate system found by rotating around the z_2 axis by the sideslip angle.

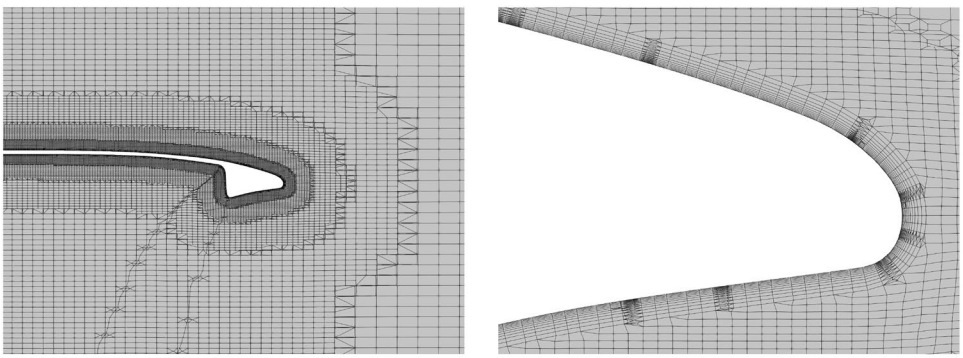

(a) (b)

Fig. 2 Illustration of computational mesh. **a** Overall grid structure. **b** lose-up of layers near disc surface

4. **Wind axes** - rotating the disc around the y_3 axis by the angle of attack, α, to obtain the coordinate system used in the CFD simulations.

The forces acting on the disc are illustrated in Fig. 3. The calculation procedure is as follows. From the initial condition, convert the velocity to the disc axes using the attitude vector,

$$\boldsymbol{u}_2 = \boldsymbol{T}_{12}(\boldsymbol{\theta})\boldsymbol{u}_1. \tag{4}$$

Note that the subscripts here corresponds to the respective coordinate system numbers, i.e. $\boldsymbol{u_1}$ is the velocity in the earth axes. Also note that the wind velocity can also be included by subtracting from the initial velocity. The sideslip angle is then found using the horizontal velocity components in the disc axes,

$$\beta = -\text{atan2}(v_2, u_2) \tag{5}$$

This angle is used to transform to the zero sideslip axes,

$$\boldsymbol{u}_3 = \boldsymbol{T}_{23}(\beta)\boldsymbol{u}_2. \tag{6}$$

The angle of attack for the disc can now be found from the velocities in this coordinate system,

$$\alpha = -\text{atan2}(w_3, u_3) \tag{7}$$

Finally, the velocity is converted to the wind axes by rotating around this angle of attack,

$$\boldsymbol{u}_4 = \boldsymbol{T}_{34}(\alpha)\boldsymbol{u}_3. \tag{8}$$

Now the forces can be calculated using the expressions in Eqs. 1 and 2 with aerodynamic coefficients from the CFD simulations. The force vector is given by

$$\boldsymbol{F}_4 = \boldsymbol{g}_4 + [-F_D, 0, F_L]^T. \tag{9}$$

Here, the gravitational force, $\boldsymbol{g}_1 = [0, 0, -mg]^T$, is also transformed to the wind axes,

$$\boldsymbol{g}_4 = \boldsymbol{T}_{14}(\boldsymbol{\theta}, \beta, \alpha)\boldsymbol{g}_1. \tag{10}$$

For the attitude vector, the trajectory model assumes a constant spin rate and only considers the roll of the disc caused by gyroscopic precession. This is a simplification assuming the disc is thrown without any wobble during the release. The roll occurs in the zero sideslip axes, hence the expression for the angular velocities is

$$\dot{\boldsymbol{\theta}}_3 = \left[-\frac{M}{\omega(I_{xy} - I_z)}, 0, 0\right]^T. \tag{11}$$

Here, the moment M is calculated using the coefficient of moment from the CFD calculation, Eq. 3. The moments of inertia, I_{xy} and I_z, are found from the geometry models. ω is the angular velocity of the disc.

These values are finally transformed back to the ground coordinate system before advancing the simulation,

$$m\dot{\mathbf{u}}_1 = \boldsymbol{T}_{41}(\boldsymbol{\theta}, \beta, \alpha)\boldsymbol{F}_4 \tag{12}$$

$$\dot{\boldsymbol{\theta}}_1 = \boldsymbol{T}_{31}(\boldsymbol{\theta}, \beta)\boldsymbol{\theta}_3 \tag{13}$$

The actual integration is performed using numerical integration routines from the `SciPy` library, more specifically using an explicit Runge-Kutta method of order 5 [21]. The full simulation code is implemented in Python and made available in the open-source sports projectile trajectory simulator Shotshaper [22], developed by the authors. The simulator has also been compared against experiments on spinning and non-spinning balls from Ref. [23], with differences in trajectory of less than 5 %. These simulations can be found in the source code.

2.4 Disc trajectory experiments

Experiments were performed by tracking the disc during actual throws. The throws are made by a player rated as an intermediate player according to the PDGA rating system [24]. The athlete gave informed consent to participate in the study, and the study was conducted in accordance with the ethical standards of the University of Stavanger and the Declaration of Helsinki [25].

Four cameras were used for the tracking, as illustrated in Fig. 4. Three of the cameras were used to estimate the release conditions of the disc, while the fourth camera was used to track the projected disc trajectory (see Online Resource 2). The back camera was placed behind the player, level with the release point of the disc, and was used for measuring the roll angle of the disc. The side camera was placed to the side of the release point, and was used to measure the pitch angle, nose angle and release velocity. The ground camera was placed below the release point, and was used to measure the spin of the disc. A straight line was drawn on the bottom plate of disc to measure the number of frames for one full revolution. These three cameras were GoPro HERO10 (GoPro Inc., California, United States) cameras with a video resolution of 2704×1520 and a frame rate of 240 FPS. The drone camera was a DJI Mini 2 (SZ DJI Technology Co. Ltd., Shenzhen, China) drone, with a resolution of 3840×2160 and a frame rate of 30 FPS. The drone was placed 100 m above the throwing field and was used to trace the 2D projected flight path of the disc. Wind velocity was measured using a Kestrel 5500 wind meter (Nielsen-Kellerman Inc., Pennsylvania, United States). The measurements and 2D path tracings were performed manually

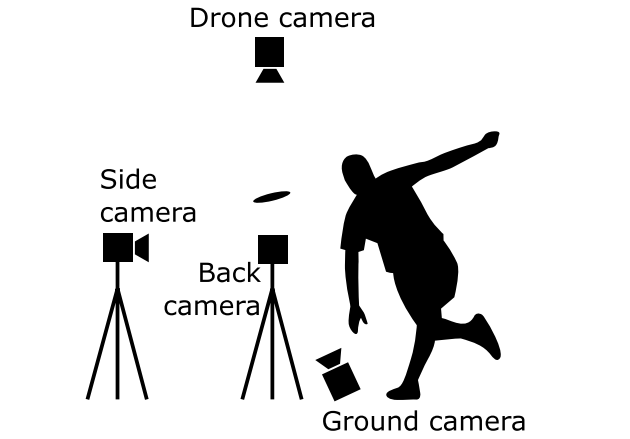

Fig. 4 Illustration of camera setup for the experiments (top), and example of traced disc trajectory from drone video (bottom)

using the open-source Tracker video analysis tool [26]. An example of the traced path is shown in Fig. 4. To estimate the uncertainty, all measurements were repeated three times, yielding the following intervals in the input parameters to the trajectory model: Disc speed $\pm 0.6\,\mathrm{m\,s^{-1}}$, roll angle $\pm 5°$, pitch angle $\pm 2°$, nose angle $\pm 2°$, yaw angle $\pm 2°$, spin rate $\pm 2°\mathrm{s}^{-1}$, wind direction $\pm 2°$ and wind speed $\pm 1\,\mathrm{m\,s^{-1}}$.

3 Results

3.1 Validation

This section presents validation tests of both the CFD model and the rigid body dynamics model. The tests were performed using the DD disc model.

3.1.1 Validation of aerodynamic coefficients

In Ref. [8], experiments were performed on non-spinning discs in a low-speed wind tunnel with a 0.9×1.1 m test section. Figure 5 compares the experimental results obtained for

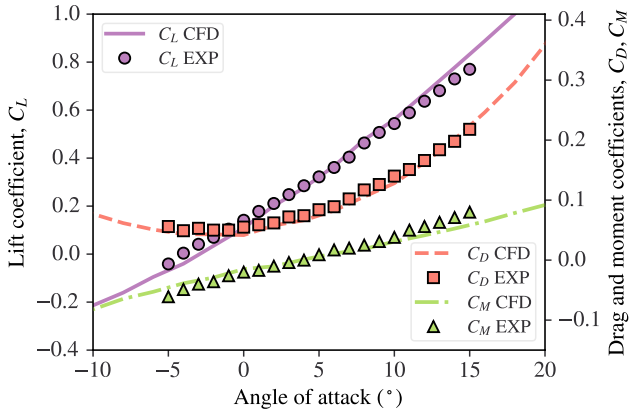

Fig. 5 Simulated aerodynamic coefficients compared with experimental results from Ref. [8] for the DD disc model

the DD model against simulated coefficients. The maximum absolute errors were 0.044, 0.013 and 0.022 for lift, drag and moment coefficients, respectively. The mean absolute errors were 4.3×10^{-4}, 6.8×10^{-3} and 3.2×10^{-3}.

3.1.2 Validation of rigid body dynamic model

Three right-handed backhand throws (with different discs of the DD model) were measured, where the athlete was asked to vary the roll angle between each throw. Invariably, it is challenging to maintain all other aspects of a throw the same, hence some differences in the other parameters were also seen. Table 1 gives the measured input parameters for the three throws. The wind was measured as a 4.8 m/s tailwind for all throws.

Figure 6 shows the trajectory of the flights viewed from above, together with the simulated trajectory (see Online Resource 3). For throw 1 and 2, the initial roll angle is high, causing the disc to track towards the left for most of the flight. Throw 3 has a lower roll angle, and the disc first drifts towards the right due to gyroscopic precession before finishing towards the left. The simulated trajectory follows the experimental trajectory well, but ends slightly earlier for all three cases. The deviation in total distance for the three throws is 13.1 m, 13.6 m and 18.9 m, respectively. To analyze the sensitivity to the input parameters, Monte-Carlo simulation for each throw were performed, where the throw

Table 1 Input parameters for disc throw experiment

Throw	Pitch (°)	Roll (°)	Speed (m s^{-1})	Spin (rad s^{-1})	Yaw (°)
1	15.5	21.8	24.7	138.0	−31.6
2	12.3	14.7	24.2	128.5	−9.60
3	5.20	−0.70	24.5	147.7	8.00

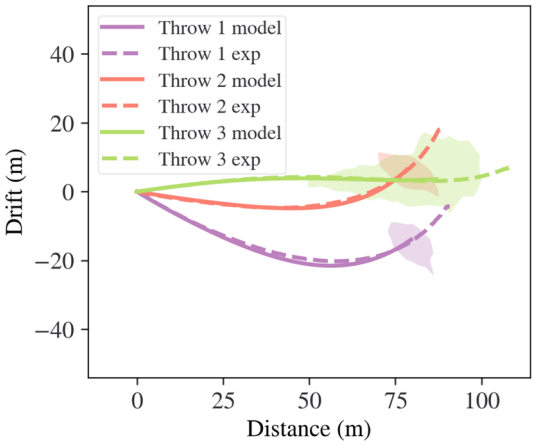

Fig. 6 Simulated flight trajectories (viewed from above) compared against experiments for three different throws with the DD model. The shaded areas indicate model sensitivity to input parameters

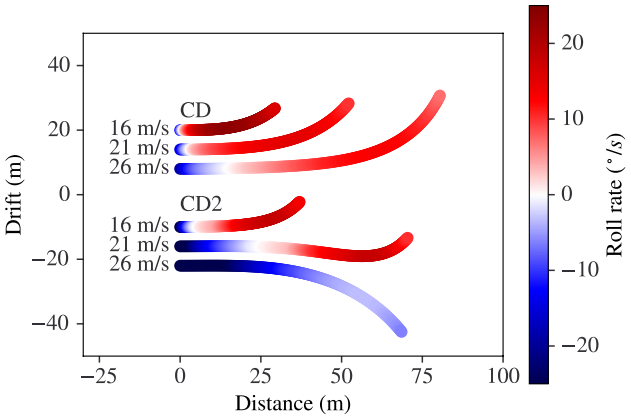

Fig. 7 Simulated flight trajectories (viewed from above), for CD and CD2 with varying launch speed

was repeated 1000 times with random sampling of the input parameters within the estimated experimental uncertainties. The shaded areas in the plot are alpha shapes calculated from all the landing spots of these throws. For throw 1 and 2, the variation in landing area is small, with a total area of 136m^2 and 156m^2, respectively. For throw 3 the variation is larger, with an area of 835m^2. This larger variation is mainly due to the lower initial pitch angle, making the shot length more sensitive to changes in the input parameters. Of all the input parameters, the variation in pitch angle and roll angle had the largest influence on the landing position, with a maximum difference in total length of about 4 m for throw 1 and 2, and 20 m for throw 3.

3.2 Comparison of discs

As an example of usage of the proposed methodology, simulations were performed comparing the flight of the CD and CD2 discs. The CD driver has a flatter top, as given by the shorter distance from the tip of the disc to the top, 0.96 cm vs 1.17 cm for CD2. The CD disc also has a more concave shape on the underside of the rim.

Figure 7 shows simulated flight trajectories for the two discs for right-handed backhand throws with three different release speeds; 16m s^{-1}, 21m s^{-1} and 26m s^{-1}. The other input parameters are roll angle 8°, pitch angle 10°, nose angle 0° and the spin rate was set to 5.2 times the release speed. For the lowest speed, the trajectory is similar for the two discs, except for an 8 m longer distance. For the middle speed, the trajectory for the CD disc is similar to the lower speed, with a steady drift towards the left. The CD2 disc, however, rolls over and starts drifting towards the right before finishing towards the left. This results in a straighter flight and a 16 m longer distance. At the highest speed the CD2 disc maintains a negative roll rate and drifts towards the right throughout the entire flight, while the CD disc maintains the consistent pattern of drifting towards the left.

The primary reason for these differences is the difference in moment coefficient, as shown in Fig. 8. Except for the lowest angles of attack, which are not seen in typical flights, the CD2 disc has a consistently lower moment coefficient than the CD disc. As given in Eq. 3, this results in a lower roll rate.

During the initial stage of the flight, the disc speed is high giving a high lift force. This makes the disc rise through the air, thereby reducing the incoming angle of attack and giving a negative roll rate, making the disc drift towards the right. Towards the end of the flight the disc slows down and starts falling, which gives a higher angle of attack and positive roll rate, making the disc turn towards the left.

These differences can be further understood from studying the flow pattern over the discs from the CFD simulations. Figure 9 shows the velocity and pressure in a slice along the flow direction through the center of the discs, for

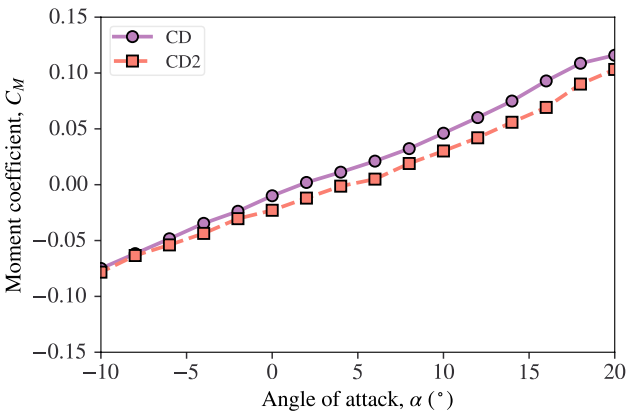

Fig. 8 Comparison of moment coefficient for CD and CD2 discs

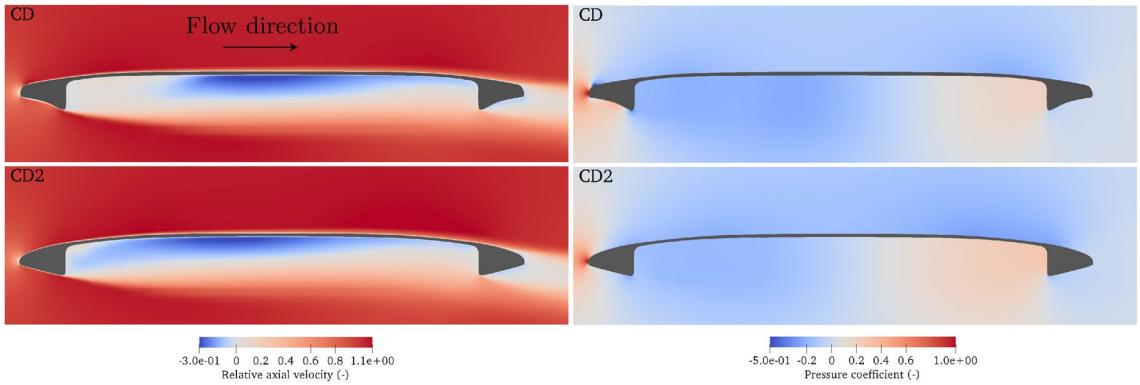

Fig. 9 Comparison of flow pattern (left) and pressure (right) for the CD and CD2 discs in a slice through the centerline of the disc in the flow direction. The flow is from left to right and the angle of attack is zero

zero angle of attack. Figure 10 shows the corresponding cumulative lift, drag and moment coefficients as a function of distance along the disc. The cumulative coefficients were calculated by dividing the disc into 50 sections along the flow direction, finding the coefficients for each section, and then successively adding these together. The final number will then be the total coefficient for the disc.

The development of lift and drag along the disc can broadly be divided into four sections as shown in Fig. 10. The first section is flow across the rim. For the CD disc, the blunter edge causes some flow separation along the underside of the rim. The flat top and concave underside also produces a lift force, and hence also a positive moment. The CD2 disc with its higher curvature of the top and a rounder underside has a negative lift in this region. Section II is characterized by a recirculation zone underneath the disc. The drag for the CD disc increases more here compared to CD2 due to the larger wake caused by the concave rim. The lift is also reduced as a result of lower pressures towards the center of the disc. In Section III the pressure starts increasing on the underside as the flow meets the rim along the back of the disc. This causes a pronounced increase in lift (and drag) and a corresponding reduction in the moment coefficient. In Section IV, the air flow separates over the back rim, which gives an increase mainly in the drag coefficient as the contribution from the top and bottom of the rim is similar in terms of lift. The drag is slightly higher for CD2 as the flow separates earlier from the top due to the higher curvature.

4 Discussion

The developed methodology showed reasonable agreement with both wind tunnel tests and trajectory experiments. However, there are still several uncertainties and limitations worth discussing.

For the CFD simulations, the CFD was not performed on the exact same geometry as used in the wind tunnel experiments. As shown earlier, there can be differences in the disc geometry due to the production techniques. The flow around a disc golf disc is also complex, with separation at the leading edge, reattachment at the bottom of the flight plate and subsequent separation and vortex formation along the sides and back of the disc. These complex interaction might require the use of scale-resolved methods such as detached eddy simulations to capture in more detail. Such methods have recently been applied to sports projectiles such as golf balls [27–29], soccer balls [30, 31] and feather shuttlecocks [32]. Transition to turbulence is also not currently accounted for in the turbulence model used.

Disc wear during use is also a factor altering the shape and aerodynamics of the disc. Some of these alterations can be captured by CFD, such as stretching of the plastic altering the overall shape of the disc. However, the influence of scratches and dents could impact the boundary layer development and transition to turbulence in ways that should be investigated in detail using experimental techniques. The benefit of using CFD is relatively rapid simulation time, and also allowing further coupling to optimization and inverse design techniques.

The trajectory model also has uncertainties associated with it. The simulated throws were slightly shorter than the experimental throws. This could indicate that the simulated lift coefficients are too low or the drag coefficients too high. The biomechanics of the throw could also have an impact on the input parameters to the trajectory model. The shape of the disc could affect the throw parameters, such as the amount of spin imparted on the disc or the off-axis torque (causing wobble). In the trajectory experiments, the biggest uncertainty is the wind environment. Repeating the experiments either in more controlled conditions or with more detailed measurements of the wind

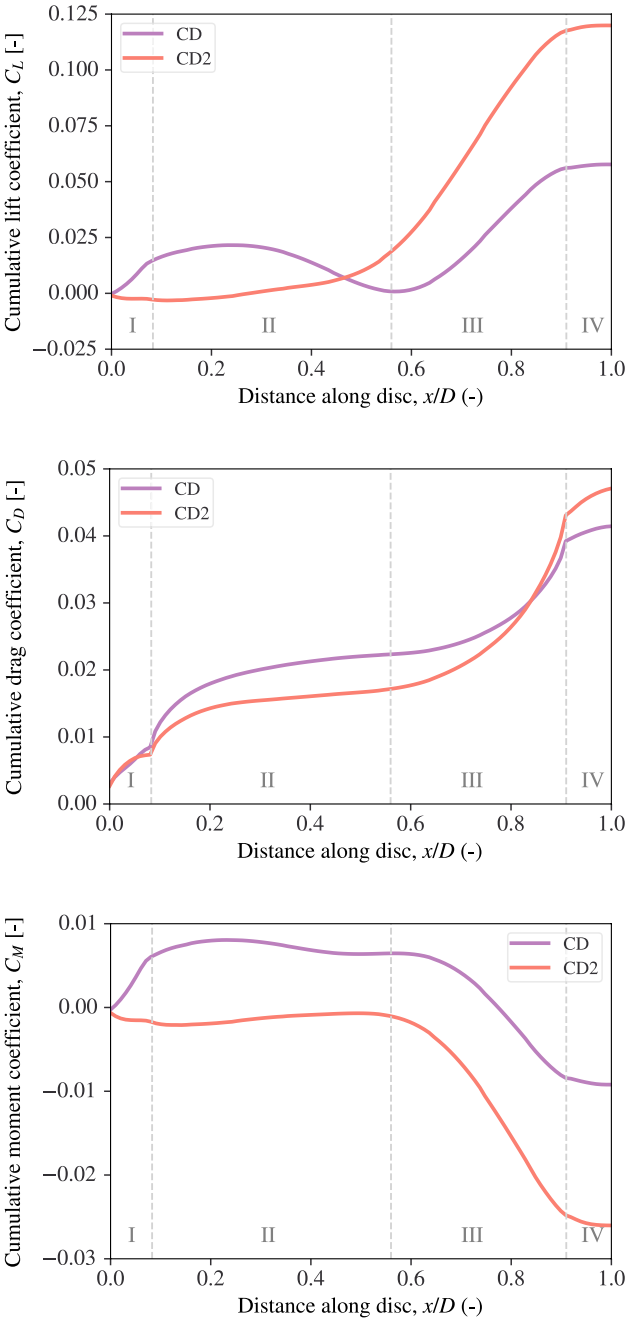

Fig. 10 Comparison of lift (top), drag (middle) and moment (bottom) coefficients for the CD and CD2 discs

would be beneficial. Also, measuring the complete 3D trajectory of the disc instead of just the projected trajectory would enable a more thorough validation of the model. A larger amount of data in terms of number of participants, discs and throws would also be a useful extension of the work.

5 Conclusion

This study presented a simulation method for disc golf trajectories combining computational fluid dynamics and rigid body dynamics. CFD simulations were used to estimate aerodynamic coefficients for the disc, which were then used in the flight trajectory model. The CFD model showed good agreement with wind tunnel tests, with mean absolute errors of 4.3×10^{-4}, 6.8×10^{-3} and 3.2×10^{-3} for lift, drag and moment coefficients, respectively. The trajectory model showed reasonable agreement with trajectory experiments, with similar flight patterns and errors in distance of less than 20%. The methodology was used to simulate two different disc types, highlighting different aspects of disc golf flight. The results illustrate how the full interaction between the aerodynamics and the dynamics are necessary to understand the flight of a disc golf disc. The presented methodology for trajectory experiments can be used to gather more data for comparing against models, and the open-source trajectory simulator can over time build up a library of discs for use in further research on disc golf flight. The simulator can also be useful for studying other projectiles in sports.

Appendix A Transformation matrices

This section defines the transformation matrices used in the rigid body dynamics model. Note that these matrices are slightly different than those presented in Ref. [15], since the z axis points upwards instead of downwards. To convert from body axes to disc axes,

$$\boldsymbol{T}_{12}(\boldsymbol{\theta}) = \begin{bmatrix} \cos\theta\cos\psi & \sin\phi\sin\theta\cos\psi - \cos\phi\sin\psi & \cos\phi\sin\theta\cos\psi + \sin\phi\sin\psi \\ \cos\theta\sin\psi & \sin\phi\sin\theta\sin\psi + \cos\phi\cos\psi & \cos\phi\sin\theta\sin\psi - \sin\phi\cos\psi \\ -\sin\theta & \sin\phi\cos\theta & \cos\phi\cos\theta \end{bmatrix} \tag{A1}$$

To convert from disc axes to zero sideslip disc axes,

$$\boldsymbol{T}_{23}(\beta) = \begin{bmatrix} \cos\beta & -\sin\beta & 0 \\ \sin\beta & \cos\beta & 0 \\ 0 & 0 & 1 \end{bmatrix} \tag{A2}$$

To convert from zero sideslip disc axes to wind axes,

$$\boldsymbol{T}_{34}(\alpha) = \begin{bmatrix} \cos\alpha & 0 & -\sin\alpha \\ 0 & 1 & 0 \\ \sin\alpha & 0 & \cos\alpha \end{bmatrix} \tag{A3}$$

Converting directly from ground axes to wind axes is done by successive multiplication of the transformation matrices, e.g.

$$\boldsymbol{T}_{14}(\boldsymbol{\theta}, \beta, \alpha)\boldsymbol{a} = \boldsymbol{T}_{12}(\boldsymbol{\theta})\boldsymbol{T}_{23}(\beta)\boldsymbol{T}_{34}(\alpha)\boldsymbol{a}. \tag{A4}$$

Also, to convert back from one axes to another, the transposed transformation matrix can be applied, e.g.

$$\boldsymbol{T}_{21}(\boldsymbol{\theta}) = \boldsymbol{T}_{12}(\boldsymbol{\theta})^T. \tag{A5}$$

Supplementary Information The online version contains supplementary material available at https://doi.org/10.1007/s12283-022-00390-5.

Funding Open access funding provided by University Of Stavanger.

Declarations

Conflict of interest The authors declare no conflict of interest. The first author is a member of the editorial board of the journal and was not involved in the double-blind peer-review process.

References

1. (2022) UDisc: The disc golf growth report. https://udisc.com/disc-golf-growth-report. Accessed 21 Apr 2022
2. (2022) PDGA: The disc golf growth report. https://www.pdga.com/news/2021-pdga-year-end-demographics-report. Accessed 21 Apr
3. Dunipace DB Flying Disc (U.S. Patent 5 531 624, Jul. 1996)
4. Hendrick EE, Flying saucer (U.S. Patent 3 359 678, Dec. 1967)
5. (2021) PDGA: Technical Standards - Manufacturer Guidelines for Obtaining PDGA Approval of Golf Discs and Targets . Technical report, PDGA
6. Potts JR (2005) Disc-wing aerodynamics. PhD thesis, University of Manchester, Manchester, UK
7. Rohde A (2000) A computational study of flow around a rotating disc in flight. Master's thesis, Florida Institute of Technology, Florida, US (December)
8. Kamaruddin N, Potts J, Crowther W (2018) Aerodynamic performance of flying discs. Aircr Eng Aerosp 90(2):390–397
9. Lukes R, Hart J, Potts J, Haake S (2014) A CFD analysis of flow around a disc. Procedia Eng 72:685–690
10. Honeycutt DB (2020) Prediction of disc wing aerodynamic characteristics using computational fluid dynamics. Master's thesis, UNC Charlotte, North Carolina, US
11. Lorenz RD (2005) Flight and attitude dynamics measurements of an instrumented frisbee. Meas Sci Technol 16:738–748
12. Lee J, Lee YJ, Sung SK, Kim K (2017) A novel flight coefficient estimation of flying disc and its performance analysis via onboard magnetometer measurement. In: 33rd AIAA Aerodynamic Measurement Technology and Ground Testing Conference, p 3237
13. Weizman Y, Tan AM, Fuss FK (2020) Measurement of flight dynamics of a frisbee using a triaxial MEMS gyroscope. In: MDPI Proceedings, vol 49, p 66
14. Hummel SA (2003) Frisbee flight simulation and throw biomechanics. Master's thesis, University of California, Davis, California, US
15. Crowther W, Potts J (2007) Simulation of a spinstabilised sports disc. Sports Eng 10(1):3–21
16. Weller HG, Tabor G, Jasak H, Fureby C (1998) A tensorial approach to computational continuum mechanics using object-oriented techniques. Comput Phys 12(6):620–631
17. Jasak H, Jemcov A, Tukovic Z, et al (2007) OpenFOAM: A C++ library for complex physics simulations. In: CMND, vol. 1000. IUC Dubrovnik Croatia
18. Menter FR (1994) Two-equation eddy-viscosity turbulence models for engineering applications. AIAA J 32(8):1598–1605
19. Warming R, Beam RM (1976) Upwind second-order difference schemes and applications in aerodynamic flows. AIAA J 14(9):1241–1249
20. Etkin B, Reid LD (1996) Dynamics of flight: stability and control, vol 3. John Wiley & Sons, Hoboken, NJ, US
21. Dormand JR, Prince PJ (1980) A family of embedded Runge-Kutta formulae. J Comput Appl Math 6(1):19–26
22. Knut Erik T (2022) Giljarhus: Shotshaper - A sports projectile trajectory simulator. https://github.com/kegiljarhus/shotshaper. Accessed 11 Apr 2022
23. Mencke JE, Salewski M, Trinhammer OL, Adler AT (2020) Flight and bounce of spinning sports balls. Am J Phys 88(11):934–947
24. (2022) PDGA: PDGA Ratings System Guide. https://www.pdga.com/ratings/guide. Accessed 11 Apr 2022
25. (2001) WMA: World medical association declaration of Helsinki. Ethical principles for medical research involving human subjects. Bull World Health Organization 79(4):373
26. Brown D, Cox AJ (2009) Innovative uses of video analysis. Phys Teach 47(3):145–150
27. Li J, Tsubokura M, Tsunoda M (2015) Numerical investigation of the flow around a golf ball at around the critical Reynolds number and its comparison with a smooth sphere. Flow Turbul Combust 95(2):415–436
28. Li J, Tsubokura M, Tsunoda M (2017) Numerical investigation of the flow past a rotating golf ball and its comparison with a rotating smooth sphere. Flow Turbul Combust 99(3):837–864
29. Crabill J, Witherden F, Jameson A (2019) High-order computational fluid dynamics simulations of a spinning golf ball. Sports Eng 22(1):1–9
30. Asai T, Nakanishi Y, Akiyama N, Hong S (2020) Flow visualization of spinning and nonspinning soccer balls using computational fluid dynamics. Appl Sci. https://doi.org/10.3390/app10134543
31. Iftikhar S, Sherbaz S, Haider Sehole HA, Maqsood A, Mustansar Z (2022) Large eddy simulation of the flow past a soccer ball. Math Probl Eng. https://doi.org/10.1155/2022/3455235
32. Hart J, Potts J, James D (2018) Comparison of turbulence modelling approaches in simulation of a feather shuttle: a porous conical bluff body. Sports Eng 21(4):465–478